Macromolecules

ARTICLE

pubs.acs.org/Macromolecules

Wrinkling Labyrinth Patterns on Elastomeric Janus Particles

A. C. Trindade,[†] J. P. Canejo,[†] L. F. V. Pinto,[†] P. Patrício,[‡,§] P. Brogueira,[⊥] P. I. C. Teixeira,[‡,§] and M. H. Godinho*[,†]

[†]Departamento de Ciência dos Materiais and CENIMAT/I3N, Faculdade de Ciências e Tecnologia, Universidade Nova de Lisboa, Caparica, 2829-516 Caparica, Portugal

[‡]Instituto Superior de Engenharia de Lisboa, Rua Conselheiro Emídio Navarro, 1950-062 Lisboa, Portugal

[§]Centro de Física Teórica e Computacional da Universidade de Lisboa, Avenida Professor Gama Pinto 2, 1649-003 Lisboa, Portugal

[⊥]Departamento de Física and ICEMS, Instituto Superior Técnico, Universidade Técnica de Lisboa, Avenida Rovisco Pais, 1049-001 Lisboa, Portugal

ABSTRACT: We describe a novel, low-cost and low-tech method for the fabrication of elastomeric Janus particles with diameters ranging from micrometers to millimeters. This consists of UV-irradiating soft urethane/urea elastomer spheres, which are then extracted in toluene and dried. The spheres are thus composed of a single material: no coating or film deposition steps are required. Furthermore, the whole procedure is carried out at ambient temperature and pressure. Long, labyrinthine corrugations ("wrinkles") appear on the irradiated portions of the particles' surfaces, the spatial periodicity of which can be controlled by varying the sizes of particles. The asymmetric morphology of the resulting Janus particles has been confirmed by scanning electron microscopy, atomic force microscopy, and optical microscopy. We have also established that the spheres behave elastically by performing bouncing tests with dried and swollen spheres. Results can be interpreted by assuming that each sphere consists of a thin, stiff surface layer ("skin") lying atop a thicker, softer substrate ("bulk"). The skin's higher stiffness is hypothesized to result from the more extensive cross-linking of the polymer chains located near the surface by the UV radiation. Textures then arise from competition between the effects of bending the skin and compressing the bulk, as the solvent evaporates and the sphere shrinks.

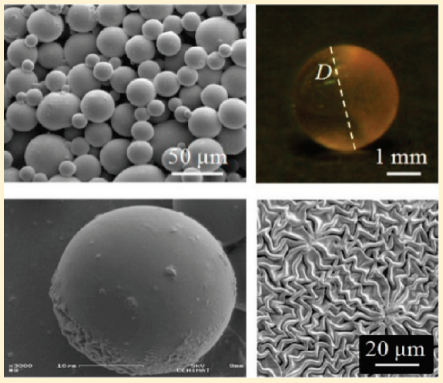

1. INTRODUCTION

Janus particles,[1] so named after the Roman god depicted with two heads facing opposite directions, likewise possess two sides with distinct compositions or surface structures. They have attracted increasing interest because of their unique properties based on additional orientational interactions and of their potential applications in a number of fields, such as optical biosensors,[2] electronic paper,[3,4] anisotropic building blocks for supra-assemblies,[5] and functional surfactants.[6] Polymers and elastomers are low-cost, lightweight, nontoxic materials that can also be used to generate a great variety of geometries, and various original approaches have been proposed for the preparation of polymeric Janus particles.[7] These include selective surface modification of symmetric particles, such as temporary masking,[8] microcontact printing,[9] partial contacting with a reactive medium,[10] based grafting polymerization at an interface,[11] and the use of directional flows or fields.[12] Ultraviolet (UV) light was also used to produce dissymmetrical surface modification of particles, derived mainly from UV absorption by photoactive compounds contained in reactant solutions or anchored to the particles, combined with light sheltering of the lower hemisphere by the upper hemisphere.[13] More recently, asymmetric colloids at an oil−water interface were also reported in the literature.[14]

An expeditious way to fabricate polymeric Janus particles would be to get some part of their surface (a hemisphere or less) to wrinkle, the remaining surface being smooth. Buckling or wrinkling of a thin film on a compliant substrate is the most common method for obtaining self-organized patterns with a wide range of morphology and complexity. Most studies performed in this field involve coating a thin hard skin on a soft elastomer sheet, such as poly(dimethylsiloxane) (PDMS), which can be expanded thermally, mechanically, or osmotically. On the other hand, we have shown that wrinkles can be produced on the surface of elastomer films[15−17] by using UV light to create a thin top layer which is much stiffer than the viscoelastic bulk material, thereby avoiding the need for complex coating or deposition steps. In all cases the length scales of these wrinkling patterns, which are typically on the order of submicrometers to tens of micrometers, are determined by the competition between the bending stiffness of the thin film on top, which penalizes short wavelengths, and the energy of stretching the substrate below, which penalizes long wavelengths.

Received: November 4, 2010
Revised: February 23, 2011
Published: March 15, 2011

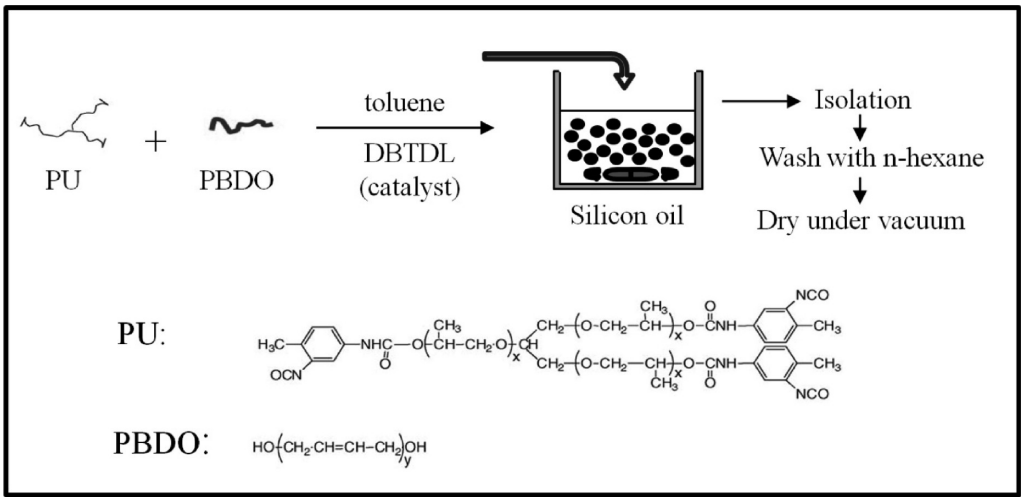

Figure 1. Preparation of poly(propylene oxide) (PU)/polybutadiene (PBDO) bisoft segment urethane/urea polymer spheres (PU, $x = 20$; PBDO, $y = 50$). The molar ratio of PU/PBDO used was 60:40. The two prepolymers were first dissolved in toluene, with a few drops of catalyst; this solution was then dripped into a silicon oil bath and stirred.

Most previous studies have been restricted to the elastic buckling patterns of planar thin films.[18−22] Some recent progress on the buckling patterns of thin films on curved compliant substrates has been summarized in a recent review.[23] The effect of sphere curvature on the critical buckling stress and wavelength was discussed, and the development of a labyrinth wrinkle pattern was also considered.[24] In particular, Cao et al.[24] demonstrated experimentally and theoretically an instance of spontaneous buckling pattern formation on spherical substrates. Using a coevaporation technique, a thin SiO_2 film a few hundreds of nanometers thick was bonded to a nearly spherical Ag substrate at high temperature for a range of substrate radii.

In this paper we describe the synthesis and experimental method to prepare urethane/urea elastomeric spheres and a simple new route for transforming them into labyrinth-wrinkled Janus particles. We are able to produce spheres with diameters ranging from tenths of micrometers to a few millimeters. The asymmetric particle wrinkling is achieved by selective UV irradiation of the spheres, followed by swelling in an appropriate solvent, and drying. No coating or deposition of any other material is involved, and the procedure is carried out at ambient temperature and pressure. The resulting Janus particle morphologies were characterized by scanning electron microscopy (SEM), atomic force microscopy (AFM), and polarizing optical microscopy (POM). We have also investigated the elastic and swelling properties of the spheres, which are crucial for the interpretation of our results. We found that the spatial periodicity of the patterns depends on particle size and polar angle (to be defined below), which affords us a remarkable degree of control over particle properties. Our results can be interpreted using different models described in the literature[18−20,23,24] for the wrinkling of a membrane on top of a soft substrate with natural curvature: we assume that each sphere consists of a thin, stiff surface layer ("skin") lying atop a thicker, softer substrate ("bulk"). The skin's higher stiffness is hypothesized to be due to the more extensive cross-linking of the polymer chains located near the surface by the UV radiation. Textures then arise from competition between the effects of bending the skin and compressing the bulk, as the solvent evaporates and the sphere shrinks. On this basis we also introduce a new model which makes closer contact with experiment and is amenable to some analytical treatment.

This paper is organized as follows. In section 2 we describe how the elastomeric Janus particles are fabricated and characterized. In section 3 we present and discuss our results: for the morphology of the unpatterned (i.e., as-made) particles (3.1), their elastic and swelling properties (3.2), and the surface modifications effected to make them into Janus particles (3.3). We next give an interpretation of the wrinkling in terms of models of a thin stiff film on top of a soft curved substrate (3.4), both as treated earlier, numerically, by others (3.4.1) and as refined and analyzed analytically by ourselves (3.4.2). We conclude in section 4 by summarizing our results and considering future directions for research.

2. EXPERIMENTAL SECTION

The elastomeric spheres were synthesized from a precursor solution composed of poly(propylene oxide)-based triisocyanate-terminated prepolymer (PU), hydroxyl-terminated polybutadiene (PBDO) (Figure 1), and a catalyst, dibutyl tin dilauryate (DBTDL), dissolved in toluene. In this work the elastomers were prepared according to the procedure described in the literature,[25,26] modified as follows. PU, purchased from Portuguese Petrochemical Industry (CPB) with a molecular weight of ∼3500 g/mol, and PBDO, as purchased from Sigma-Aldrich and consisting of a mixture of *cis* and *trans* isomers, with a number-average molecular weight of 2800 g/mol, prepolymers were dissolved in toluene (solid content 40 wt %) and one drop of catalyst was added. A weakly cross-linked urethane network was obtained, after 30 min, from chemical reaction of the cyanate end groups of PU with the hydroxyl end groups of PBDO, under a nitrogen atmosphere at room temperature. The resulting viscous solution (before gel point) was poured into a 1 mL syringe (corresponding to a diameter of 4.5 mm) fitted with a 18-gauge needle (inner diameter 0.84 mm), which was then placed on an infusion syringe pump (model KDS100) to control the polymer drip rate. The solution was dripped into a stirred silicon oil bath, the stirring speed (w) of which was adjusted to yield the desired range of sphere diameters (D). The resulting spheres were allowed to cure in the bath for at least 4 h. After that, the small elastomeric spheres could be isolated, washed with *n*-hexane, and then dried under vacuum for a few hours. Micrometer-sized particles were resuspended in water by bath

sonication, separated, extracted in hexane and washed using repeated centrifugation and redispersion steps, and then dried at 70 °C for 36 h. A Soxhlet apparatus was used to extract the spheres in toluene for 36 h at 60 °C.

The swelling properties of the spheres were determined by immersing the elastomeric particles in water, in toluene, and in a toluene−water biphase. The elastic properties of the spheres, either unswollen (dry) or swollen (wet) in toluene, were assessed by dropping the spheres from a certain height (z) normal to a hard solid surface at room temperature. The free fall trajectories of the particles were recorded with a Casio Exilim EX-F1 CCD video camera. The energy loss was determined from the maximum height of the successive bounces and averaged over six successful measurements.

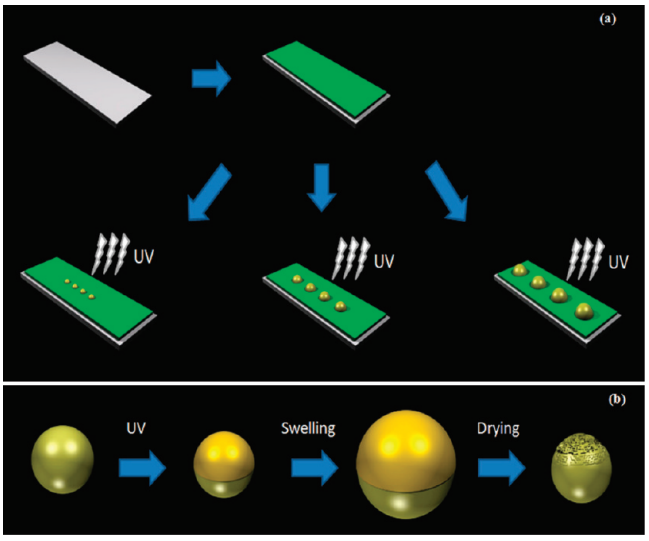

Figure 2. Schematics of the Janus particle fabrication method. (a) The polyurethane/polybutadiene (PU/PBDO) macro- and microspheres are deposited on an opaque soft cellulosic film and UV irradiated. (b) The wrinkling labyrinth patterns of asymmetric elastomeric particles appear after swelling the particles in toluene and drying them.

The Janus particles were obtained by using the general method schematized in Figure 2. The strategy adopted to modify one hemisphere without altering the surface of the other was to temporarily mask the hemisphere to be left unmodified during UV-irradiation (λ = 254 nm) for 24 h (Figure 2a). In order to shield one of the hemispheres, the precursor particles were deposited onto a solid opaque cellulosic soft substrate of controllable thickness. After removing the cellulosic substrate, the elastomeric spheres were released, washed and dried. Figure 2b shows the different steps involved in the production of the wrinkled half-sphere surface. The particles were swollen in toluene for 36 h and then dried in an oven at 70−80 °C for at least 72 h.

Optical microphotographs (obtained by POM) were taken with an Olympus (model BH) polarizing microscope equipped with a photographic camera (Olympus model Camedia C5060). The topographical features of the spheres were imaged by scanning electronic microscopy (SEM) using a SEM DSM962 model from Zeiss. Gold was deposited on the spheres by sputtering in an Ar atmosphere, using a 20 mA current, for 30 s at a deposition rate of 3 Å s^{-1}. Images were captured for an acceleration voltage of 5 kV. A D3100 with a Nanoscope IIIa controller from Digital Instruments (DI) was used for the atomic force microscopy (AFM) measurements, carried out in tapping mode under ambient conditions with a commercial tapping-mode etched silicon probe (from DI) and a 90 μm × 90 μm scanner.

3. RESULTS AND DISCUSSION

3.1. Particle Production and Characterization. The starting point of this work was the attempt to broaden the materials basis for producing spontaneous buckling patterns on spherical substrates and thereby fabricate micrometer- and millimeter-sized Janus particles. Therefore, we started by preparing spherical elastomeric particles from a solution of two prepolymers in a common solvent, to which a catalyst was added (Figure 1a),

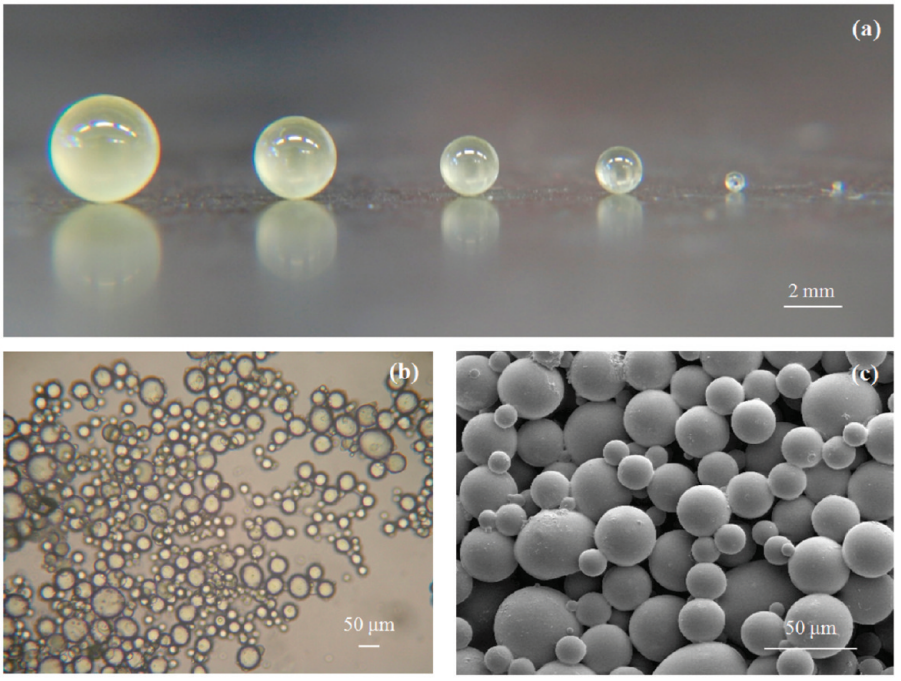

Figure 3. Spheres of different diameters can be produced by varying the stirring speed: (a) optical photographs of spheres with diameters ranging from 0.34 to 4 mm (no stirring); (b) POM and (c) SEM images of spheres with diameters ranging from 0.1 to 50 μm (stirring speed $w \approx 400$ rpm).

dx.doi.org/10.1021/ma1025169 |*Macromolecules* 2011, 44, 2220–2228

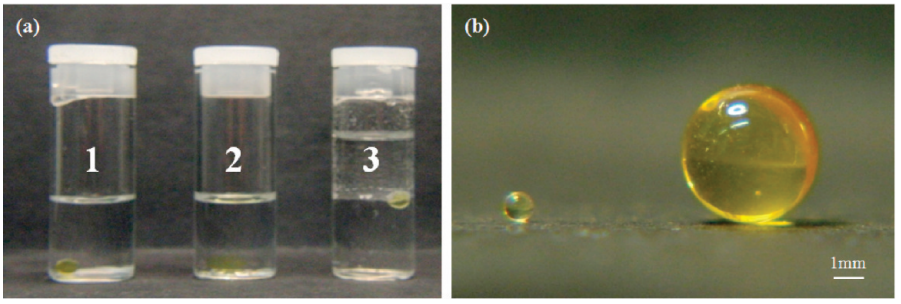

Figure 4. Swelling properties of elastomeric spheres. (a) Distribution of elastomeric spheres in water (1), toluene (2), and in a toluene−water biphase (3). The particles sink to the bottom of the vessel in (1) and (2), i.e., in either solvent, owing to the higher particle density (ρ = 1.5 g/cm^3). However, because the elastomer swells differently in each solvent (the degree of swelling in toluene is 220.0 ± 2.5%, in water it is 2.0 ± 0.5%), the particles are located at the interface in a toluene−water biphase (3). (b) Photograph of a sphere (initial diameter 0.9 mm), before and after, the swelling in toluene.

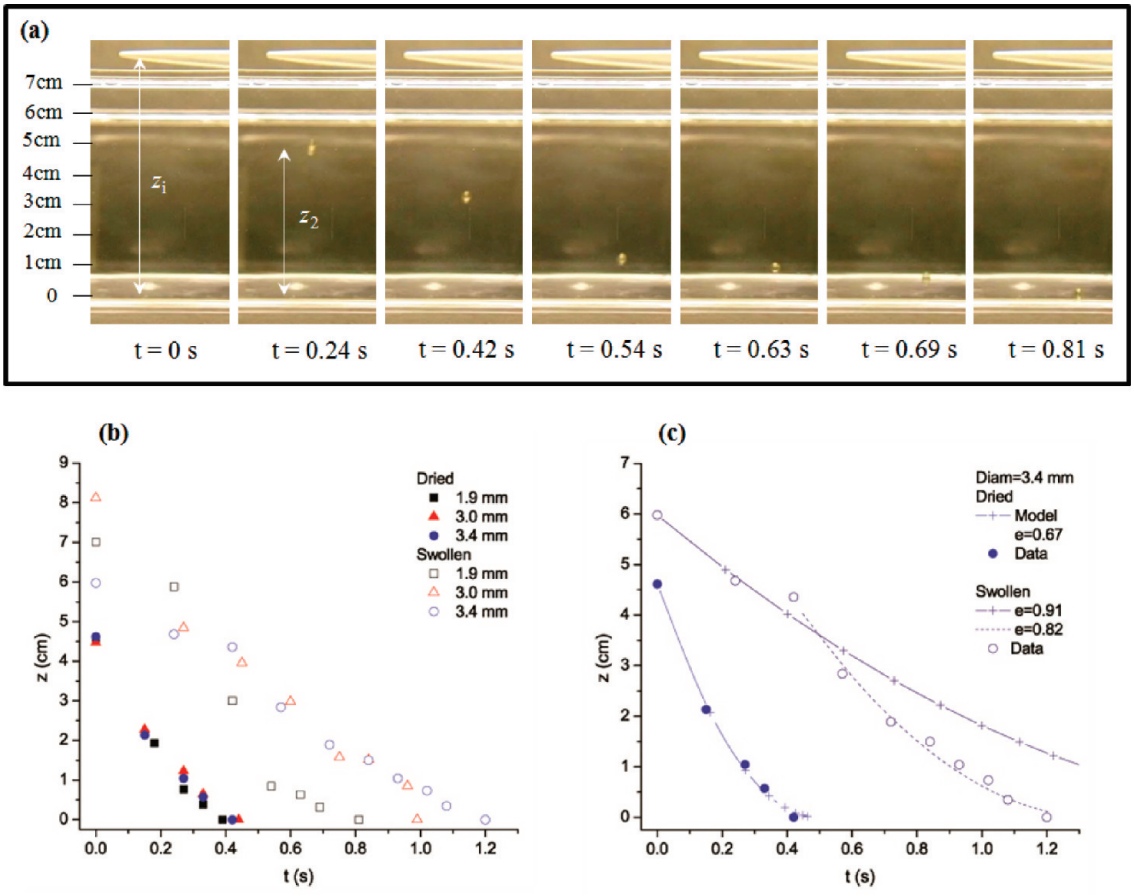

Figure 5. (a) Example of a sequence of bounces for the swollen elastomeric sphere (dry diameter D = 3.4 mm), z_i is the initial drop height and z_2 is the height of the first bounce. (b) Bouncing properties of swollen and dried particles, quantified by energy loss as a function of time (the error is less than 5%). (c) Free fall model (lines) allows the calculation of e, the restitution coefficient (defined in the text) from the fit of the maximum height of successive bounces (dry diameter D = 3.4 mm), either dried (filled symbols) or wet (open symbols); for the swollen particle two regimes can be clearly seen, corresponding to the loss of solvent during bounces (90% of all toluene lost is lost in the first two bounces).

allowing the reaction between the end groups of polybutadiene-diol (PBDO) and polyurethane (PU). This proceeds until the solution is poured into a nonsolvent system and the elastomer precipitates, forming a sterically stabilized sphere. In this step, the residual toluene diffuses into the silicon oil and the particles sink to the bottom of the vessel.

The choice of a suitable solvent/nonsolvent system is crucial for this process. In this case silicon oil proved to be suitable as the nonsolvent. We therefore followed different procedures depending on the particle size range desired. Millimeter-sized particles were produced by dropwise addition of different volumes of the reactive solution into a nonstirred silicon bath, whereas for micrometer-sized particles the silicon bath stirring speed (w) was tuned, for example, for D = 0.1−50 μm; $w \approx$ 400 rpm. After sorting, washing, and drying the millimeter-sized particles (D = 4−0.34 mm) (Figure 3a) look "shiny" and slightly yellowish,

dx.doi.org/10.1021/ma1025169 |*Macromolecules* 2011, 44, 2220–2228

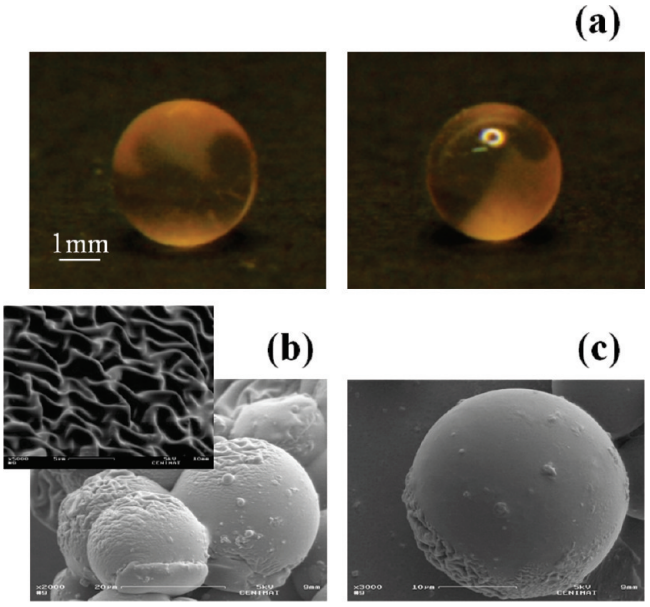

Figure 6. Millimeter- and micrometer-sized Janus particles: (a) photographs showing a millimeter-sized sphere ($D = 2$ mm), with two different surfaces (light scattering and smooth). (b) and (c) are SEM images of micrometer-sized particles showing a smooth and a wrinkled surface. The inset shows a SEM picture with detail of the wrinkled pattern.

which suggests that their surfaces are smooth. This was confirmed by SEM imaging. The micrometer-sized particles also appeared smooth, as can be seen in Figure 3b and in the corresponding SEM image (Figure 3c).

3.2. Swelling and Elastic Properties of the Particles. As will be seen later, the swelling and elastic properties of the elastomeric spheres are crucial for producing the Janus particles. Swelling was investigated by immersing them in water, in toluene, and in a toluene−water biphase (Figure 4a). We also show an image of a same sphere before and after swelling in toluene (Figure 4b). In both solvents the particles sink to the bottom of the vessels (Figure 4a, vessels 1 and 2) because the elastomeric material is denser (ρ = 1.5 g/cm^3) than either solvent. In a water−toluene biphase, however, the particles were found to reside at the interface between the two solvents (Figure 4a, vessel 3). This can be explained on the basis of the different swelling of the spheres in either solvent. The degree of swelling ($\varepsilon = (R_{swollen} - R_{initial})/R_{initial}$) of the elastomer is around 220% in toluene (see Figure 4b) and 2% in water: polybutadiene segments have a very low degree of swelling in water, and consequently we can assume that the swelling of the network in water was essentially due to the polyurethane moieties. Similar swelling results were obtained for urethane/urea polymer free-standing films.[26] Because of the higher affinity of the network for toluene, it swells as it moves through the toluene-rich phase and before coming into contact with the water; each sphere will thus have higher toluene content and therefore be repelled away from the water.

The elasticity of the swollen and dried particles was investigated through the movement analysis of their bouncing (Figure 5a shows an example of a sequence of frames) and interpreted by means of a free-fall model motion in the vertical direction, assuming a gravity acceleration of g = 9.81 m/s^2 and neglecting air friction. The inelastic collision of the falling sphere with the horizontal rigid surface is described through the normal restitution coefficient, $e = (z_i/z_{i-1})^{1/2}$, where z_i is the height of the ith bounce. The impact time was a negligible fraction of the overall duration of motion. Results for the dried sphere are well described assuming a restitution coefficient, e = 0.67. However, for the swollen sphere, two regimes were observed: one for the first two collisions, with e = 0.91, and another for the subsequent collisions, with e = 0.82. This suggests that a large fraction of the solvent is lost (by being squeezed out of the sphere) in the first two collisions, and indeed, inspection of the video recording confirms that about 90% of all toluene lost is lost in the first two bounces. These results indicate that the precursor (i.e., not yet surface-modified) particles are elastic spheres which do not lose their elasticity when swollen in toluene and that the solvent can be easily removed from the network, with a consequent reduction of the restitution coefficient. In other words, the swollen sphere is more like an elastomeric hard sphere.

3.3. Janus Particle Fabrication and Characterization. The main purpose of this work was the production of Janus particles with one smooth hemisphere and one labyrinth-wrinkled hemisphere. These asymmetric spheres were produced by selective exposure to UV radiation in the presence of oxygen. After UV irradiation the free surfaces of the spheres showed a flat topography, similar to those of the spheres not exposed to UV. In order to generate wrinkle patterns on the UV-irradiated hemispheres, the particles were first allowed to swell in a good solvent, up to their state of maximum swelling. This was followed by drying; the experimental conditions used were chosen taking into account previous results for flat films.[26] UV irradiation combined with exposure to oxygen led to oxidation and cross-linking of the PU/PBDO chains in the outer surface region, forming a hard skin on the elastomer. When this film was swollen above a critical stress and allowed to shrink (after solvent

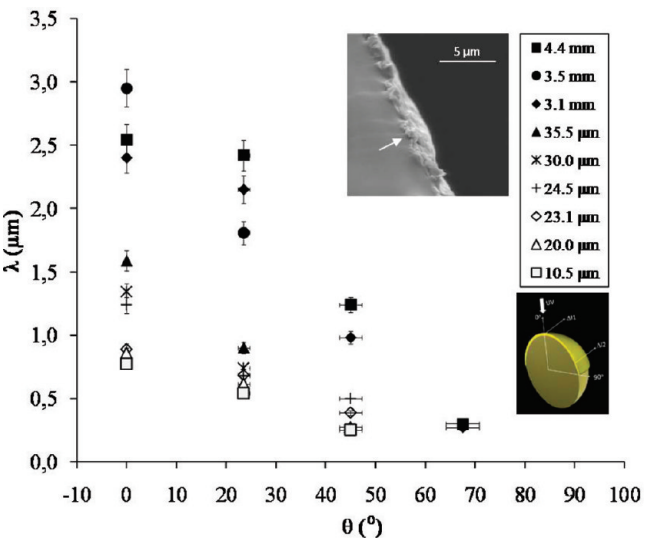

Figure 7. Large length scale wrinkle wavelength, λ, vs polar angle θ (defined in smaller inset scheme), from SEM images. The wavelength decreases on going from "polar" to "equatorial" regions. The outer layer thickness was found to vary with θ, and for particles with different diameters the following pairs of average values were obtained from SEM images after breaking the spheres in liquid nitrogen: (0°; ∼0.6 μm), (22.5°; ∼0.4 μm), (67.5°; ∼0.2 μm). The larger inset shows a cross section of a millimeter-sized sphere near θ = 67.5°; the white arrow points at the stiff outer layer.

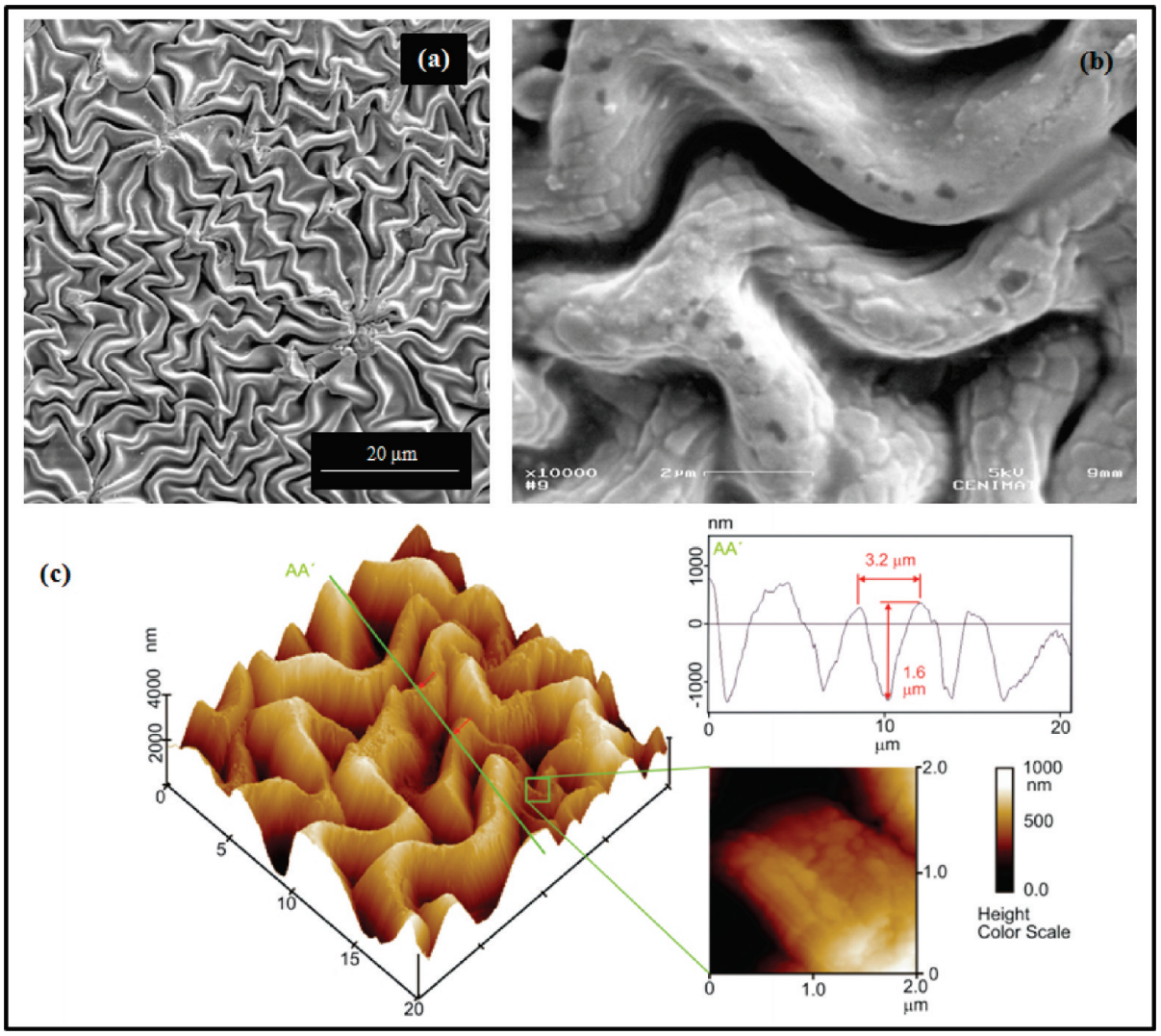

Figure 8. (a) Wrinkling wavelength, λ, obtained from SEM image of a Janus sphere with a diameter of 4.4 mm. (b) Higher magnification of the SEM image, showing the presence of smaller length scale features. (c) AFM, 3D topography image ($20 \times 20\ \mu m^2$ scan) of the rough surface at the north pole of the sphere. This surface is corrugated, with micrometer-sized features along all axes. The AA′ cross section was taken along the line marked on the 3D image. A magnification of the green square in the AFM image shows smaller length scale features.

removal), wrinkle patterns appeared on the UV-irradiated surface. Results are shown in Figure 6.

Spheres with diameters in the millimeter range (see Figure 6a) clearly exhibit two different hemispheres, one shiny and one translucent; the latter, which scatters light more strongly, is the UV-irradiated surface. These spheres were observed by SEM, and the images revealed a wrinkled labyrinth pattern of long corrugated, randomly distributed, line-like textures. The same pattern was also found for smaller micrometric particles (Figure 6b,c and SEM inset). The wrinkle wavelength, λ, on the micrometric particles was found to depend upon the wrinkle position on the sphere as parametrized by the polar angle, θ, measured relative to the direction of irradiation. At the top of the sphere (surface exposed to the UV irradiation), $\theta = 0°$ and the effect is prominent, disappearing at the equator, where $\theta = 90°$ (see Figures 6 and 7). As will be discussed in more detail in section 3.4, this is likely a consequence of the varying thickness of the stiff outer film, which is maximal at the pole and minimal (approaching zero) at the equator (see schematic representation in the inset of Figure 7). These data were confirmed by measuring the stiff film thickness (h) of broken spheres with different diameters (see Figure 7 and inset) by SEM. Because the thickness depends on θ, we were able to find the ratio between the sphere radius, R, and h, not only for different particles but also for the same particle as a function of the wrinkle wavelength, λ.

From AFM and SEM images (Figure 8), it was found that smaller wavelength features were also produced inside the larger wavelength ones. These observations suggest that the mechanism driving wrinkle formation could be the same as was proposed for the flat free-standing films described in the literature.[18]

3.4. Interpretation of the Wrinkling. In order to explain the wrinkling, we propose the following scenario. When the spheres are swollen in toluene, both the inner (soft) core and the outer (stiffer) shell deform by the same amount. The outer surface of the spheres thus remains smooth. However, when toluene is extracted, the elastomer network will contract. The inner core has a lower cross-linking density and will shrink, due to the loss of

dx.doi.org/10.1021/ma1025169 |*Macromolecules* 2011, 44, 2220–2228

solvent and sol fraction (unreacted prepolymer blocks), whereas the outer shell, which is more densely cross-linked, will preserve its dimensions. This leads to a buildup of internal stress, which is compressive for the thin outer shell and dilational for the thick inner core. Because the spheres were swollen in toluene, which is a very good solvent, they are above the critical stress for wrinkling.[24] The wrinkle wavelength will be determined by the competition between the bending stiffness of the thin outer shell (which penalizes short wavelengths) and the bulk elastic energy of core deformation (which penalizes long wavelengths). This model of wrinkling due to differential deformation was originally proposed by Bowden et al.[18] for a stiff film atop a soft (planar) substrate and predicts that the wrinkle wavelength should scale as

$$\lambda \sim h(E_h/E_s)^{1/3} \quad (1)$$

where E_h and E_s are respectively the Young's moduli of the "hard" film and the "soft" substrate and h is the film thickness, assumed to be much smaller than that of the substrate.

3.4.1. Analysis Using Cao et al.'s Model. More recently,[24] the mechanism of spontaneous wrinkling pattern formation in thin films on curved substrates was addressed numerically and successfully applied experimentally to micrometer-sized particles consisting of a SiO_2 film/Ag spherical substrate assembly of radius R. Cao et al.[24] showed that the wrinkle wavelength scales in this case as $\lambda/R = a(R/h)^b$, with $a = 3.0$ and $b = -0.8$, for a given range of particle sizes ($R/h < 50$) and material parameters. For larger particles, they obtained a wrinkle wavelength in reasonable agreement with the planar analytical result.

We fitted our data for a comparable range of micrometer-sized elastomeric particles to this same equation and obtained almost the same exponent: $b = -0.82$. The fit and the experimental data are plotted in Figure 9. However, our experimental geometry, although similar, is not exactly the same as that of ref 24. In our system the outer shell is not closed but covers only half of the sphere. Moreover, the shell thickness changes with the polar angle θ (see Figures 6 and 7). In both curved geometries, the same trend is observed: the wrinkle wavelength is affected by the substrate curvature for the smaller micrometer-sized particles, while for larger millimeter-sized particles λ becomes insensitive to R/h. The value of $a = 0.89$ obtained in our fit, smaller than that of Cao et al.,[24] reflects not only a different geometry but also different ratios of Young's moduli, lower for the elastomeric spheres ($(E_h/E_s)_{elast} = 1.4$, from mechanical testing of free-standing elastomeric films[26]) than for the SiO_2/Ag particles ($(E_h/E_s)_{SiO_2/Ag} = 3.0$).[24]

3.4.2. Simple Analytical Model. Whereas the effect of curvature has been addressed in a few numerical studies of thin films on spherical[23,24,28] or cylindrical[23,29] substrates, to our knowledge only one paper has reported more detailed analytical calculations, for the case of a cylindrical substrate with a stiff outer ring.[30] A simplified plane-strain ring-foundation model was used to obtain an exact solution for the wrinkle wavelength, which should scale as

$$\lambda \sim h(R/h)^{1/4}(E_h/E_s)^{1/4} \quad (2)$$

in certain particular elastic regimes. In their model, Yin et al.[30] consider a ring subjected to an external "fluid" line pressure (constrained to remain normal to the ring during deformation), which in turn compresses a softer elastic foundation. Their total potential energy comprises the external potential, responsible for the external pressure; a simplified elastic energy for the foundation, which depends only on the radial displacement of its external surface and is proportional to a constant foundation stiffness; and, finally, the elastic energy of the ring, which contains

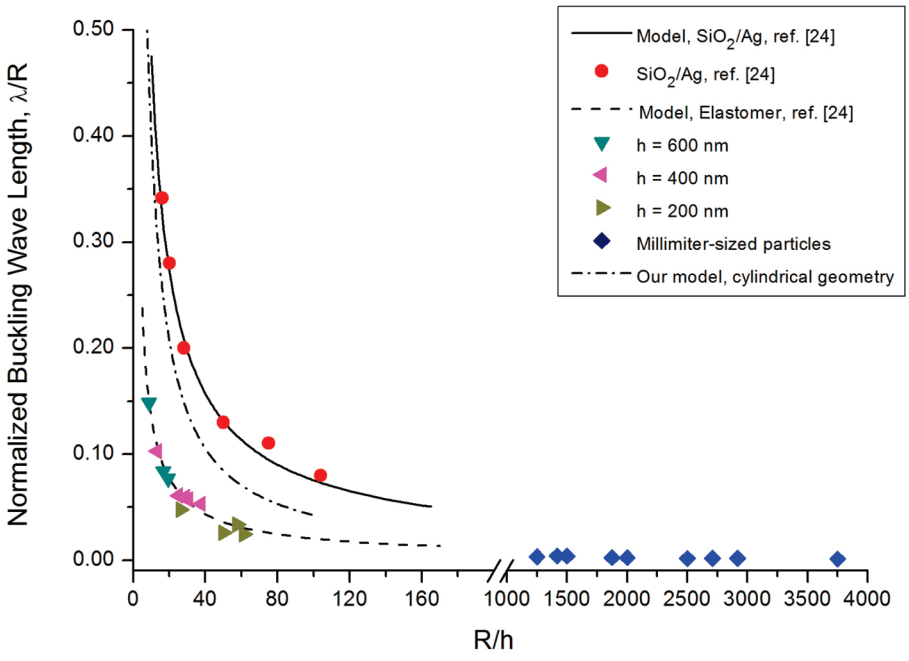

Figure 9. Results for the normalized wrinkle wavelength, λ/R, as a function of R/h, for micrometer- and millimeter-sized particles. The layer thickness, h, was varied either by exploring regions with different polar angles, θ, within a single sphere, or by considering different spheres. Data for the system SiO_2/Ag from ref 24 are also plotted in order to compare the two systems. Our data for micrometer-sized elastomeric particles were fitted to the equation $\lambda/R = a(R/h)^b$, also used by Cao et al.,[24] yielding $a = 0.89$ and $b = -0.82$. The dash-dotted curve is the prediction of our model for a cylindrical geometry, and $(E_h/E_s)_{elast} = 1.4$.

stretching and bending terms and allows for radial and circumferential displacements of the ring.

Here, we derive a similar, but different, simplified elastic model for a curved cylindrical substrate with a stiff skin and a soft core. We do not assume any external pressure but consider the elastic deformation imposed by the soft core on the hard skin, as in the actual experimental system. Initially (i.e., before drying), both skin and core have radius R_0; upon solvent removal, the equilibrium core radius becomes smaller, $R < R_0$. This deformation can be expressed as

$$\varepsilon = \frac{R_0 - R}{R} \tag{3}$$

We write the elastic energy as a sum of both soft core and hard skin contributions:

$$F = F_s + F_h \tag{4}$$

In our model, we consider the whole elastic energy of the soft core, i.e., the energy density integrated over the whole volume of the cylinder, but we neglect circumferential or longitudinal (along the cylinder axis) deformations. Hence, we denote the elastic displacement field as $\mathbf{u} = u(r,\theta)\hat{\mathbf{e}}_\mathbf{r}$, with $\hat{\mathbf{e}}_\mathbf{r}$ the unit vector along the radial direction, and the elastic energy of the (shrunken) soft cylinder writes

$$F_s = \frac{E_s}{2(1+\nu_s)} \int \left[\left({u_r}^2 + \left(\frac{u}{r}\right)^2 + \frac{{u_\theta}^2}{2r^2} \right) + \frac{\nu_s}{1-2\nu_s} \left(u_r + \frac{u}{r} \right)^2 \right] \mathrm{d}V \tag{5}$$

We assume that the outer skin does not suffer any plastic deformation, as is usually the case with stiffer materials. As stated above, the skin will be under a compressive stress exerted by the soft core. Now the elastic energy of compressing a thin plate scales with its thickness, h, and is therefore much larger than its bending energy, which scales with h^3. Therefore, we assume the skin can only bend, which gives

$$F_h = \frac{E_h h^3}{24(1-{\nu_h}^2)} \int (k - k_0)^2 \, \mathrm{d}A \tag{6}$$

where $k_0 = 1/R_0$ and $k = k(\theta)$ are respectively the curvatures of the undeformed and deformed skin, to which the soft core remains attached throughout. In eqs 5 and 6, ν_s and ν_h are the Poisson's ratios of respectively the soft core and the stiff skin.

We expand $u(r,\theta)$ in a Fourier series and minimize the total elastic energy, eq 4 with eqs 5 and 6, subject to the constraint that the outer skin must preserve its original perimeter, $2\pi R_0$. To leading order in ε, we obtain (noting that to this order k_0 is unimportant and may be set equal to zero):

$$F = \frac{L_z \pi \varepsilon E_s R^2}{a(1+\nu_s)} \sum_{n=1}^{\infty} \frac{1}{n^2} \left[\left(\sqrt{1+an^2} + (1-2a) \right) + \frac{a(1+\nu_s)}{6(1-{\nu_s}^2)} \frac{E_h}{E_s} \frac{h^3}{R^3} (1-n^2)^2 \right] \tag{7}$$

where L_z is the length of the cylinder and $a = (1-2\nu_s)/2(1-\nu_s)$. For large $n = 2\pi R/\lambda$, the elastic energy of the soft core scales with $1/n$ and that of the shell scales with n^2, whence we recover Bowden et al.'s result for the planar film (eq 1). However, for intermediate values of n there is a new term in the elastic energy of the inner core, which scales with $1/n^2$ and by itself would yield eq 2, thereby suggesting that λ should be a (weakly) increasing function of R. Note that this very same result was derived in ref 30. Our simple model exhibits the same qualitative behavior displayed by our experimental results: the wrinkle wavelength λ is an increasing function of R/h that saturates to a constant value at large R/h ($R/h > 100$), in qualitative agreement with the experimental data of Figure 9 and consistent with the finite-element (FEM) calculation reported in Figure 6 of ref 24. Both Yin et al.'s model[23] and our model (for a cylinder) predict $\lambda/R \sim (R/h)^{-0.75}$ for $R/h < 50$, whereas in Cao et al.'s model (for a sphere) the exponent is -0.8. Our simple analytical model also establishes a connection between the two different scaling law predictions for the wrinkle wavelength, one valid for small cylinder radius R/h and the other for large R/h. Our model prediction for λ/R vs R/h is shown as the dash-dotted curve in Figure 9, for $(E_h/E_s)_{elast} = 1.4$ and $\nu_s = \nu_h = 0.4$. Two remarks are in order. First, the behavior is qualitatively the same as for a sphere. Second, for a given E_s/E_h, λ for a cylinder is greater than for a sphere, in agreement with Figure 6 in ref 23.

Our very preliminary analytical results for the sphere suggest that, if we allow the outer shell to be open, there may exist inextensional wrinkling modes of the outer shell that are periodic in the azimuthal angle ϕ, giving rise to a "parasol" or "star" pattern when viewed from a position above the "north pole" of the sphere. Interestingly, and encouragingly, these would likely be similar to the "star defects" seen in Figure 7a and also found numerically by Cao et al.[23,28] In between "stars", it is possible to observe a texture that is reminiscent of the zigzag Miura-ori pattern observed in a drying slab of gelatin with a thin skin under biaxial compression.[31] These theoretical treatments are underway and will be published elsewhere.

4. CONCLUSIONS

In this paper we describe a very simple method to fabricate spherical asymmetric (Janus) particles from a single elastomeric material. Particles with diameters ranging from tenths of a micrometer to a few millimeters can be fabricated. The asymmetry is generated by selectively UV-irradiating one-half of the elastomeric spheres, followed by swelling and drying in a good solvent. The synthesis and particle preparation are straightforward and use current chemicals and methods: no sophisticated deposition or emulsification steps are necessary as spheres are made of a single elastomeric material, and all steps are performed at ambient temperature and pressure. The topographies ("wrinkles") generated on the surfaces of the spheres possess amplitudes on the order of 1 μm, and wavelengths ranging from a few hundred nanometers to a few micrometers. These are easily controllable by varying the particle diameter, layer thickness, and degree of swelling. The surface-induced wrinkles have their origin in the UV-induced changes at the molecular level in the top surface layer of the irradiated hemisphere. We found that for millimeter-sized spheres the wrinkling wavelength dependence on material properties is described by a theoretical model proposed for flat elastic films.[18,32] Taken together, macro- and microparticles allow determination of the dependence of the wrinkling wavelength upon particle curvature: in the micrometer range, the wrinkle wavelength is an increasing function of particle radius, which is in agreement both with Cao et al.'s results and the predictions of our analytical model. The micrometer-sized elastomeric particles seem to follow the same quantitative trends as the Ag core/SiO_2 shell system analyzed in the literature.[20,23,24] This is evidence that similar phenomena can be obtained in completely different systems. Finally, it appears fitting to note that we have been able to fabricate particles named after Janus,

the Roman god of doorways and passages, which exhibit labyrinthine patterns.

■ ACKNOWLEDGMENT

This research was supported by the Portuguese Science and Technology Foundation through grants SFRH/BD/37958/2007, SFRH/BPD/64330/2009, project PTDC/CTM/099595/2008, and pluriannual contracts with CENIMAT/I3N, ICEMS, and CFTC.

■ REFERENCES

(1) de Gennes, P. G. *Science* **1992**, *256*, 495.
(2) Himmelhaus, M.; Takei, H. *Sens. Actuators, B* **2000**, *63*, 24.
(3) Millman, B. K., Jr.; Prevo, B. G.; Velev, O. D. *Nature Mater.* **2005**, *4*, 93.
(4) Fialkowski, M. B. A.; Grzybowski, B. A. *Nature Mater.* **2005**, *4*, 93.
(5) Hong, L.; Cacciuto, A.; Luijten, E.; Granik, S. *Nano Lett.* **2006**, *6*, 2510.
(6) Binks, B. P.; Fletcher, P. D. I. *Langmuir* **2001**, *17*, 4708.
(7) Walther, A.; Muller, A. H. E. *Soft Matter* **2008**, *4*, 663.
(8) Paunov, V. N.; Cayre, O. J. *Adv. Mater.* **2004**, *16*, 788.
(9) Cayre, O.; Paunov, V. N.; Velev, O. D. *J. Mater. Chem.* **2003**, *13*, 2445.
(10) Bradley, J. C.; Ma, Z. *Angew. Chem., Int. Ed.* **1999**, *38*, 1663.
(11) Zhang, J.; Jin, J.; Zhao, H. Y. *Langmuir* **2009**, *25*, 6431.
(12) Takei, H.; Shimizu, N. *Langmuir* **1997**, *13*, 1865.
(13) Liu, L.; Ren, M.; Yang, W. *Langmuir* **2009**, *25* (18), 11048.
(14) Park, B. J.; Furst, E. M. *Langmuir* **2010**, *26* (13), 10406.
(15) Godinho, M. H.; Figueirinhas, J. L.; Zhao, C.-T.; de Pinho, M. N. *Macromolecules* **2000**, *33*, 7675.
(16) Godinho, M. H.; Melo, L. V.; Brogueira, P. *Mater. Sci. Eng., C* **2003**, *23*, 919.
(17) Efimenko, K.; Rackaitis, M.; Manias, E.; Vaziri, A.; Mahadevan, L.; Genzer, J. *Nature Mater.* **2005**, *4*, 293.
(18) Bowden, N.; Brittain., S.; Evans, A. G.; Hutchinson, J. W.; Whitesides, G. W. *Nature* **1998**, *393*, 148.
(19) Cerda, E.; Mahadevan, L. *Phys. Rev. Lett.* **2003**, *90*, 074302.
(20) Genzer, J.; Groenewold, J. *Soft Matter* **2006**, *2*, 310.
(21) Guvendiren, M.; Yang, S.; Burdick, J. A. *Adv. Funct. Mater.* **2009**, *19*, 3038.
(22) Singamaneni, S.; McConney, M. E.; Tsukruk, V. V. *Adv. Mater.* **2010**, *22*, 1263.
(23) Chen, X.; Yin, J. *Soft Matter* **2010**, *6*, 1217.
(24) Cao, G.; Chen, X.; Li, C.; Ji, A.; Cao, Z. *Phys. Rev. Lett.* **2008**, *100*, 036102.
(25) Zhao, C. T.; de Pinho, M. N. *Polymer* **1999**, *40*, 6089.
(26) Godinho, M. H.; Trindade, A. C.; Figueirinhas, J. L.; Melo, L. V.; Brogueira, P.; Deus, A. M.; Teixeira, P. I. C. *Eur. Phys. J. E* **2006**, *21*, 319.
(27) Park, M.; Harrison, C.; Chaikin, P. M.; Register, R. A.; Adamson, D. H. *Science* **1997**, *276*, 1401.
(28) Yin, J.; Cao, Z.; Li, C.; Sheinman, I.; Chen, X. *Proc. Natl. Acad. Sci. U.S.A.* **2008**, 10519132.
(29) Yin., J.; Chen, X. *J. Phys. D: Appl. Phys.* **2010**, *43*, 115402.
(30) Yin, J.; Chen, X.; Sheinman, I. *J. Mech. Phys. Solids* **2009**, *57*, 1470.
(31) Mahadevan, L.; Rica, S. *Science* **2005**, *307*, 1740.
(32) Genzer, J.; Groenewold, J. *Soft Matter* **2006**, *2*, 310.